RSC Advances

PAPER

View Article Online
View Journal | View Issue

Cite this: *RSC Adv.*, 2020, **10**, 26494

Temperature–humidity dual regulation of a single-core–double-shell microcapsule fabricated by electrostatic-assembly and chemical precipitation†

Xueyan Hou,[ab] Qianqian Li,[a] Zehui Yang,[a] Yuqi Zhang, *[ab] Wenbo Zhang[b] and Ji-Jiang Wang [a]

Humidity and temperature control materials have attracted increasing attention due to their energy saving and intelligent regulation of human comfort in the field of interior building and clothing. Phase change microcapsules have been widely used, however, most of which focus on temperature regulation without humidity control. In this work, we report a novel temperature–humidity dual regulation microcapsule with single-core–double-shell structure. FT-IR and XRD measurements confirmed that the shell materials were successfully fabricated on the paraffin core *via* electrostatic-assembly and the subsequent chemical precipitation method. SEM, TEM and optical microscope photos showed that the microcapsules were spherical morphology with layer-by-layer shells at a diameter around 2–5 μm. The SiO_2 shell was aggregated from nano-sized particles and formed a loose and porous micro-structure, supported by the result of N_2 adsorption–desorption isotherms. In addition, the synergistic effect of hydrophilic and porous loose (chitosan/GO/chitosan)–SiO_2 double shells endowed the microcapsules with humidity regulation. The constructed microcapsules showed temperature regulation behavior due to its phase change performance of paraffin and good thermal durability after 10 thermal cycles. They also showed stable humidity regulation performance after repeated adsorption/desorption. The simulation experiments of temperature and humidity regulation indicated that the microcapsule could keep the temperature and humidity in a stable range. The as-prepared microcapsules have outstanding temperature and humidity regulation properties, showing an application prospects in energy-saving fields.

Received 20th April 2020
Accepted 9th July 2020

DOI: 10.1039/d0ra03554h

rsc.li/rsc-advances

Introduction

With the growing demand for human thermal-humidity comfort, controlling of environmental temperature and humidity is very important in many fields, such as building materials,[1,2] textiles.[3] It has been reported that temperature and humidity control material can reduce heating and cooling energy consumption.[4] Microencapsulation is an effective strategy to provide phase change materials with a shapely characteristic and can increase the area of heat transfer.[5,6] The microencapsulated phase change materials have been applied in energy storage, waste heat recovery and targeted pollutant removal.[7] Core–shell phase change microcapsules have extensively developed to regulate the environmental temperature by shells modification to improve thermal conductivity, stability and reduce leakage. This is because the physicochemical and mechanical properties of shell determines the heat transportation efficiency and durability of phase change microcapsules.[8,9] The conventional shell materials contain organic,[10,11] inorganic[12–15] and organic–inorganic composite.[16,17] For example, a paraffin-based phase change microcapsule with SiO_2 shell achieved high encapsulation efficiency, good latent heat storage and thermal stability.[18] However, the leakage of phase change material core, which is very important to the durability of phase change microcapsules in practical application, cannot be prevented effectively by the conventional shell. Therefore, it is urgently needed to modify the shell to improve the performance of phase change microcapsules.

Graphene oxide (GO) sheets have been reported as a barrier to modify the shell of microcapsule to reduce the leakage of phase change materials.[19,20] Furthermore, GO can simultaneously improve thermal conductivity and encapsulation capacity[19,21,22] due to their good thermal conductivity and large specific area.[23,24] Although the phase change microcapsules containing GO show the temperature regulation with low leakage, the humidity regulation cannot be achieved well. Microcapsules containing porous inorganic minerals, natural polymers, or hydrophilic

[a]*Key Laboratory of New Energy & New Functional Materials, Shaanxi Key Laboratory of Chemical Reaction Engineering, College of Chemistry and Chemical Engineering, Yan'an University, Yan'an, Shaanxi, 716000, PR China. E-mail: yqzhang@iccas.ac.cn*
[b]*Shaanxi Collaborative Innovation Center of Industrial Auxiliary Chemistry & Technology, Shaanxi University of Science & Technology, Xi'an, Shaanxi, 710021, PR China*

† Electronic supplementary information (ESI) available. See DOI: 10.1039/d0ra03554h

polymers[25–27] have been used for the humidity regulation, such as the reported microcapsules composed of palmitol–palmitic acid–lauric acid core and SiO_2 shell.[28]

Actually, a desirable microcapsule should have both the performance of temperature–humidity regulation and low leakage. Efforts have been devoted to mix phase change materials with hygroscopic or porous inorganic materials[2,28–30] to achieve dual regulation of temperature and humidity. This strategy requires high compatibility of phase change materials and hygroscopic materials, and good stability of composite materials. However, simple mixture of two materials with different performance can not be able to display their respective functions well. For core–shell phase change microcapsules, phase change core and hydrophilic or/and porous shell are utilized to regulate temperature and humidity, respectively. The phase change core needs dense shell as a barrier to prevent leakage, while humidity regulation requires porous shell to adsorb/release moisture. The contradictory for the shell structures confines the development of core–shell phase change microcapsules with temperature–humidity dual regulation. Therefore, it is still a great challenge for the integration of temperature and humidity regulation and low leakage into one core–shell microcapsule.

In this work, we constructed a microcapsule with a single core and double shells *via* electrostatic-assembly and the subsequent chemical precipitation to achieve both temperature–humidity dual regulation and low leakage. The multifunctional microcapsules were composed of paraffin core for temperature regulation, chitosan–GO–chitosan inner shell as a barrier for low leakage and hydrophilic porous SiO_2 outer shell for humidity regulation. The as-prepared microcapsules showed outstanding temperature and humidity regulation with low leakage, indicating a good application prospect in the energy storage and humidity control. It provides a strategy for solving the contradictory of shell structure between humidity and temperature regulation in one microcapsule.

Experimental

Materials and characterization

Liquid paraffin was provided by Tianjin Fuyu Fine Chemical Co. Ltd. Solid paraffin (melting point, 58 °C) was provided by Shanghai Hualing Rehabilitation Equipment Factory. Span-80, Tween-80, chitosan, and glutaraldehyde were acquired from Hefei Bomei Biotechnology Co. Ltd. Graphene oxide (GO, thickness 0.335–1.2 nm, diameter 300–500 nm, 1–2 layer) was provided by Suzhou Tanfeng Technology Co., Ltd. The other reagents were purchased commercially and used as received. Ultra-pure MilliQ water (18.2 mΩ cm) was used in all of the experiments.

Optical microscope photos were obtained with an optical microscope (SA3300) for all the samples which were successively washed with petroleum ether and distilled water several times. Scanning electron microscopy (SEM) measurements were performed on a FEI Verous 460 high-resolution scanning electron microscope after spraying Pt. Transmission electron microscopy (TEM) images were obtained with a Tecnai G2 F20 S-TWIN TMP field emission transmission electron microscope. The samples were dispersed in ethanol ultrasonically for 10 min. N_2 adsorption–desorption isotherms were measured with a Micro-Active ASAP 2460 isothermal nitrogen sorption analyzer. The surface area and pore size distribution were obtained by BET analysis and BJH method, respectively. The chemical composition of microcapsules was analyzed using a Bruker Vertex 70 Fourier Transform Infrared (FT-IR) spectroscope over a scanning range of 400 to 4000 cm^{-1}. X-ray diffraction (XRD) patterns were obtained from a Bruker D8 diffractometer, in a scanning range of 5–50°, at a rate of 5° min^{-1}. The thermal conductivity of microcapsules was measured by transient plane source method (Hot Disk, TPS 2500). Phase change properties and thermal durability with 10 thermal cycles were tested by differential scanning calorimeter (DSC, TA Q2000) in the temperature range of 0–70–0 °C at a heating/cooling rate of 5 °C min^{-1}.

Preparation of microcapsules

Chitosan was added to 2 wt% of acetic acid to form 20 mg mL^{-1} of chitosan solution. GO of 50 mg was ultrasonically dispersed in 50 mL of distilled water for 30 min to prepare the GO suspension of 1 mg mL^{-1}.

Solid paraffin (2.5 g) and liquid paraffin (2.5 g) were mixed and melted at 60 °C in a three-necked flask to obtain liquefied paraffin. Emulsifier composed of Span-80 (0.18 g) and Tween-80 (0.36 g) was dispersed in distilled water (25 g) and added into the three-necked flask, followed by stirring at 500 rpm for 1 h to emulsify. Then, 20 mL of chitosan solution (20 mg mL^{-1}), X mL GO suspension (1 mg mL^{-1}, X = 0, 3, 5, 7 mL) and 20 mL of chitosan solution were successively dropped into the three-neck flask at intervals of 10 min, followed by crosslinking with 0.12 g of glutaraldehyde for 10 min. Sodium silicate solution of 4 mol L^{-1} (12 mL) was poured into the mixture, stirring for 10 min, followed by dropwise adding NH_4Cl solution of 1.5 mol L^{-1} (60 mL) into the mixture and stirring 3 h at 60 °C. Finally, the resulting microcapsules were washed with petroleum ether to remove the free paraffin and then with water to eliminate the soluble substance, followed by pumping filtration and drying in an oven at 40 °C for further characterizations. The as-prepared microcapsules by using 0 mL, 3 mL, 5 mL and 7 mL of GO were denoted as GO-0, GO-3, GO-5 and GO-7, respectively.

Leakage ratio

The microcapsule samples ($m_0 \approx 0.2$ g) were placed on filter papers and moved into an oven at 50 °C to test leakage ratio. After 24 h, the samples were taken out to weigh the mass (m_1). The leakage ratio can be calculated by the following equation:

$$\text{Leakage ratio} = \frac{m_0 - m_1}{m_0} \times 100\%$$

Adsorption/desorption of moisture

Adsorption/desorption of moisture was performed according to GB/T20313-2006/ISO. Different relative humidity (RH) condition was obtained from saturated salt solution in a desiccator.

RH of 32%, 57%, 75%, 84% and 97% were provided by the supersaturated solution of $MgCl_2 \cdot 6H_2O$, NaBr, NaCl, KCl and K_2SO_4 at 25 °C, respectively.

Adsorption of moisture. Under different relative humidity, the microcapsules of ~0.2 g was put into an opening weighing bottle and then moved into a desiccator under the specified conditions of temperature and humidity. After a certain time, the microcapsules were weighed and the obtained mass was recorded as m_s. The test was stopped until m_s kept constant, in which case the moisture content was equilibrium moisture content. The moisture adsorption rate was calculated as follows:

$$\text{Moisture adsorption rate} = \frac{m_s - 0.2}{0.2} \times 100\%$$

Desorption of moisture. The moisture-saturated microcapsules under RH of 97% were tested for moisture desorption in a desiccator at 25 °C and 32% of RH. The initial mass of dry microcapsules was ~0.2 g. The total mass of moisture-saturated microcapsules (RH = 97%) was recorded as m_t. The moisture-saturated microcapsules were put into the desiccator for a certain time and then were weighed as m_d. The moisture desorption ratio was calculated as follows:

$$\text{Moisture desorption rate} = \frac{m_t - m_d}{m_t - 0.2} \times 100\%$$

Moisture adsorption/desorption stability. 0.2 g of samples were alternately placed in the environment with relative humidity of 32% and 97%. After being stored for 24 hours, the samples were weighed to calculate the moisture content of the samples. 10 cycles were carried to evaluate the moisture adsorption/desorption stability.

The temperature and humidity regulation in simulated environment

A 200 mL small container containing sample GO-5 (2 g) was placed in a desiccator with simulated changing temperature and relative humidity, then the temperature and humidity in the small container were recorded by a hygrothermograph. The blank group without sample was performed under the same condition.

Results and discussion

Preparation and characterization

The microcapsules were designed as single core and double shells. Scheme 1 shows the synthesis process of microcapsules, including paraffin emulsification, electrostatic assembly of GO and chitosan, and chemical precipitation of SiO_2 shell. The mixed paraffin composed of solid and liquid paraffin at a mass ratio of 1 : 1 was emulsified in Span 80/Tween 80 aqueous solution, resulting in a stable oil-in-water (O/W) emulsion (Scheme 1a). This O/W emulsion was good for the assembly of hydrophilic chitosan on the surface of paraffin micelle. Thus, the positively charged chitosan was facilely captured on the surface by the interaction between chitosan and hydroxyl

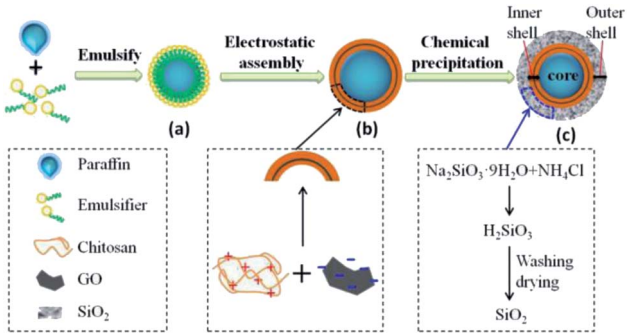

Scheme 1 Schematic illustration of the preparation for the single-core–double-shell microcapsules. The paraffin was first emulsified to form O/W paraffin micelle (a) as a core of the microcapsule. Positively charged chitosan and negatively charged GO were then layer-by-layer assembled by electrostatic interaction on the surface of paraffin micelle. The chitosan/GO/chitosan were covered on the paraffin microcapsule and acted as an inner shell (b). Finally, SiO_2 was precipitated on the surface of the inner shell as an outer shell *via* the reaction between sodium silicate and ammonium chloride solution (c). Core: paraffin, inner shell: chitosan/GO/chitosan, outer shell: SiO_2.

groups of emulsifiers. The negatively charged GO (at pH of 7.0 (ref. 31)) was then electrostatically assembled on the chitosan,[32,33] followed by a second electrostatic assembly of chitosan (Scheme 1b). As a result, this layer-by-layer assembly of chitosan solution and GO suspension formed a chitosan/GO/chitosan inner shell on the paraffin micelle. Finally, sodium silicate and ammonium chloride solution were added and precipitated[17] on the surface of the inner shell to form a SiO_2 outer shell (Scheme 1c). Herein, the hydrophilic emulsion micelles of paraffin (O/W) were employed to combine hydrophilic chitosan with positive charge, followed by electrostatically assembly of GO with negative charge to form the chitosan/GO/chitosan inner shell. The inner shell was then covered by porous and hydrophilic SiO_2 outer shell *via* chemical precipitation. This kind of synthesis route ensured the single-core–double-shell structure of the microcapsules.

We fabricated several microcapsules containing different contents of GO. The optical microscope photos of the freshly prepared microcapsules are shown in Fig. 1. Clearly, the core–

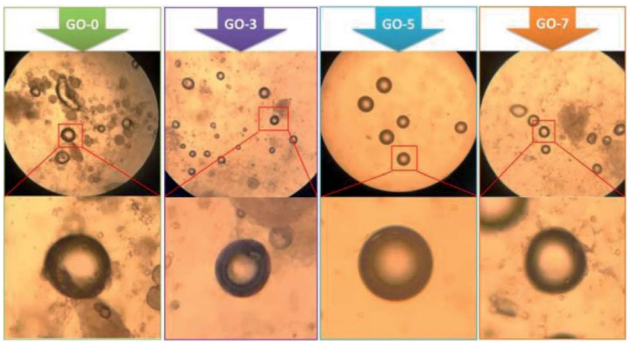

Fig. 1 Optical microscope photos of the freshly prepared core–shell microcapsules (taken at magnification of 10× eyepiece and 16× objective lens).

shell structure could be seen easily. For all the samples from GO-0 to GO-7, the core was light-transmitting because the paraffin did not completely cool down and solidify when microcapsules were freshly prepared.[34] Multiple layer-by-layer shells could be found in the magnified view of the microcapsules GO-3, GO-5 and GO-7, indicating that the electrostatic assembly of chitosan/GO/chitosan and precipitation of SiO_2 shell has been occurred successfully.

The surface morphology of the as-prepared microcapsules was characterized by SEM, as shown in the top of Fig. 2. The prepared microcapsules were about 2–5 μm. The precipitated SiO_2 nanoparticles aggregated on the surface of the spherical microcapsules. TEM images in the middle and bottom of Fig. 2 exhibit the spherical microcapsules and obvious core–shell structure, especially for GO-5 and GO-7. The darker part of the sphere was the paraffin core and the outer light-colored layer was the shell. The size of core–shell microcapsules was in the range of 2 μm and 5 μm, which was also consistent with the results of SEM. It is hard to distinguish the border between the chitosan and GO in the TEM micrographs, owing to the low content of GO. This is different from the clear layer-by-layer shell in the optical microscope photos (Fig. 1), which can be attributed to the wet/dry state of samples. The samples for optical microscope test were wet. In this case, both GO and chitosan in shell were wet and expanded, thus it is easier to observe the interface between them. In contrast, the samples for TEM were dry and the layer-by-layer shell could not be seen clearly. In addition, the SiO_2 shell could be distinguished from the light-colored outermost layer with loose microstructure. GO can not be seen in the TEM images due to the low contents. The chitosan/GO inner shell acted as a barrier to reduce leakage and the SiO_2 outer shell was to regulate humidity. Compared with the paraffin core and SiO_2 outer shell, the content of GO is small, therefore, it is difficult to distinguish the double-shell from the SEM and TEM.

Nitrogen adsorption testing was performed to further investigate the pore structure of the SiO_2 outer shell, as shown in Fig. 3. The N_2 adsorption/desorption isotherms (Fig. 3a) show

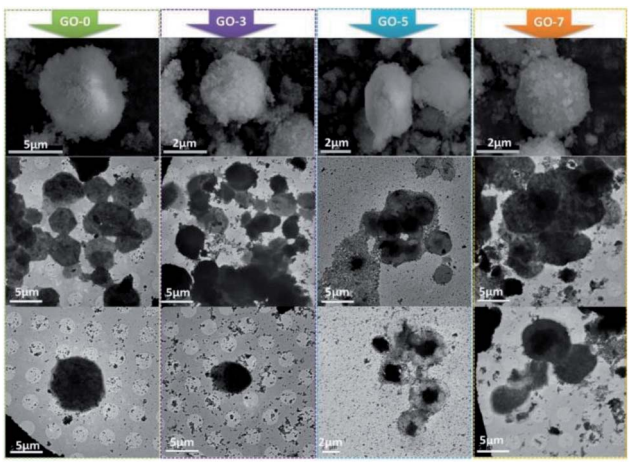

Fig. 2 SEM (the top) and TEM (the middle and bottom) images of the prepared microcapsules.

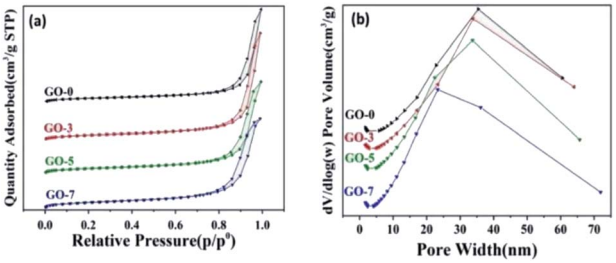

Fig. 3 (a) N_2 adsorption/desorption isotherms and (b) pore width distribution curves.

that the adsorption curves of the as-prepared microcapsules accorded with type-IV isotherms according to the IUPAC adsorption isotherm system.[35] The N_2 isotherms shows a capillary condensation step at $p/p^0 = 0.75$–1.0, in which a type-H3 hysteresis loop occurred, demonstrating a loose aggregation of SiO_2 nanoparticles and forming a hierarchical porous architecture of the SiO_2 outer shell. Fig. 3b demonstrates that the pore sizes were distributed in the range of 5–70 nm for the prepared microcapsules. The maximum of pore volumes appeared when the pore sizes were 35.4, 33.8, 33.7 and 23.3 nm for GO-0, GO-3, GO-5 and GO-7, respectively. The porosity parameters of microcapsule samples were shown in Table 1. The corresponding BET surface area was 89.36, 113.48, 112.86 and 133.96 $m^2\ g^{-1}$, demonstrating that the introduction of GO clearly increased the surface area of the microcapsules. Their average pore sizes were 33.19, 30.19, 26.33 and 21.82 nm, which were in accordance with the results in Table 1. The results proved that the average pore sized decreased with an increase in GO content, suggesting that a larger inner shell could decrease the pore size and increase the surface area of SiO_2 nanoparticles in the outer shell. On the other hand, the residual GO, which was not assembled in the inner shell, would be mixed with the subsequent addition of sodium silicate to participate in the formation of silica shells. The presence of such small-sized GO in SiO_2 shell will result in smaller pore volume and larger surface area.

Summarizing the results of SEM, TEM and N_2 adsorption, we can find that the loose and porous SiO_2 shell was formed *via* the aggregation of nano-scale silica particles during the chemical precipitation process of sodium silicate. The mesoporous structure and large surface areas in SiO_2 shell will be conducive to moisture adsorption and give microcapsules humidity performance.

The chemical composition was characterized by FT-IR and XRD. FT-IR spectra of paraffin, chitosan, GO, SiO_2, and

Table 1 The porosity parameters of the microcapsule samples

Samples	BET surface area ($m^2\ g^{-1}$)	Average pore size (nm)	BJH adsorption cumulative volume of pores ($cm^3\ g^{-1}$)
GO-0	89.36	33.19	0.75
GO-3	113.48	30.19	0.86
GO-5	112.86	26.33	0.74
GO-7	133.96	21.82	0.72

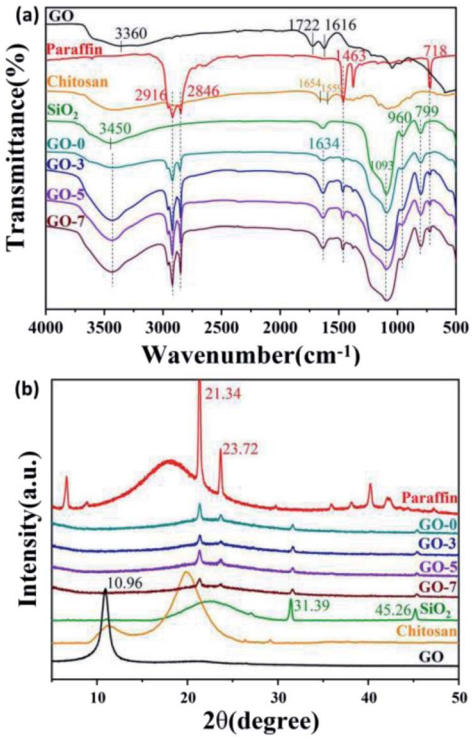

Fig. 4 (a) FT-IR spectra and (b) XRD patterns of paraffin, GO, chitosan, SiO_2 and the prepared microcapsules including GO-0, GO-3, GO-5 and GO-7.

microcapsules including GO-0, GO-3, GO-5 and GO-7 are shown in Fig. 4a. The FT-IR spectrum of paraffin shows the stretching vibration of $-CH_2-$ at 2916 cm^{-1} and 2846 cm^{-1}. The bending vibration peaks of $-CH_2$ were located at 1463 cm^{-1} and 718 cm^{-1}. Additionally, the typical peak of $(CH_2)_n$ ($n \geq 4$) belonged to paraffin could be observed at 718 cm^{-1}.[36] From the IR spectrum of GO, it can be seen that GO contains hydrophilic groups (–OH, COOH, and C=O). The peaks of –OH and the absorbed water molecules were observed around 3360 cm^{-1}. The peaks at 1722 cm^{-1} and 1036 cm^{-1} could be assigned to the stretching vibration of C=O and C–O–C in aryl carboxylic acids, respectively. The peak at 1616 cm^{-1} was the stretching vibration of C=C in GO.[37] For the spectrum of SiO_2, a broad band around 3450 cm^{-1} was attributed to the stretching vibration of Si–OH. The peak at 960 cm^{-1} belongs to the Si–OH bending vibration. The characteristic peaks at 1093 cm^{-1} and 799 cm^{-1} were arisen from the stretching vibration of Si–O–Si.[15,38] For the FT-IR of chitosan, there are obvious amide I and II bands at 1654 and 1559 cm^{-1}, respectively.[39] In the spectra of microcapsules with different GO contents, the peaks at 3360, 2916, 2846, 1463, 718, 960, 1093 and 799 cm^{-1}, indicated that GO, paraffin and SiO_2 have been introduced into the microcapsules successfully. For the microcapsules containing GO (GO-3, GO-5 and GO-7), the stretching vibration peak (~3360 cm^{-1}) of O–H in carboxyl group from GO was obviously stronger than that of the microcapsules without GO (GO-0). We found the peaks at 1654 and 1559 cm^{-1} of chitosan could not be observed clearly due to its low contents and the overlap of the adjacent peaks. Simultaneously, a new enhanced peak at 1634 cm^{-1} occurred.

The crystallinity of paraffin, chitosan, GO, SiO_2 and the as-prepared microcapsules were investigated *via* XRD and the patterns are shown in Fig. 4b. All of the microcapsules exhibited the profiles of paraffin at $2\theta = 21.34°$ and 23.72°, the profiles of SiO_2 at $2\theta = 31.39°$ and 45.26°, indicating that the encapsulated paraffin maintained its original crystal structure[36] and SiO_2 have been introduced in the microcapsules. However, the characteristic patterns of GO at 10.96° (ref. 40) and amorphous patterns of chitosan around 20° could not be observed obviously in the microcapsules due to their lower contents.

Phase change performance

The temperature regulation of the as-prepared microcapsules was studied *via* measuring phase change temperature and latent heat. Here, the paraffin in core was composed of solid and liquefied paraffin as the mass ratio of 1 to 1. Therefore, the melting point of mixed paraffin was lower than that of the solid paraffin. Fig. 5a and b shows the DSC curves of mixed paraffin and microcapsules, including GO-0, GO-3, GO-5 and GO-7. Clearly, the microcapsules and paraffin exhibited similar phase change process. Only one melting peak (downward) and crystallization peak (upward) could be observed, indicating the solid–liquid melting or liquid–solid crystallization of paraffin. This phase change property of microcapsules was caused by paraffin in the core, which proved that paraffin had been successfully encapsulated in the microcapsules. The melting peak of microcapsule samples were wider than that of the paraffin, which means they need more time to finish the melting process,[41] because the heat must transfer through the shell layer.

In Fig. 5c, the melting temperature peaks of GO-0, GO-3, GO-5 and GO-7 were 38.18, 37.65, 40.5 and 37.67 °C, respectively, which were all lower than that of paraffin (44.33 °C). Similarly, the crystallization temperature peaks of GO-0, GO-3, GO-5 and GO-7 were also lower than 47.81 °C of paraffin and they were 43.12, 43.37, 45.25, and 44.18 °C, respectively. The crystallization temperatures were higher than melting temperatures for

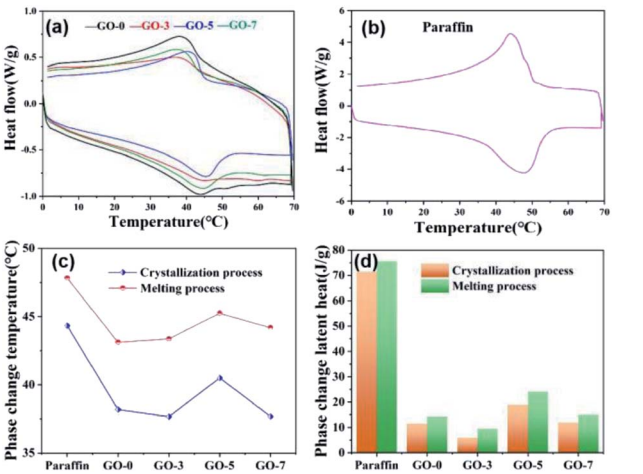

Fig. 5 DSC curves of (a) microcapsules and (b) paraffin, and (c) their phase change temperatures and the (d) corresponding latent heats.

all of the samples. The difference between the melting and crystallization temperatures is commonly defined as supercooling degree, which is often used to determine the supercooling level of phase change materials.[42] Notebly, microencapsulation increased the supercooling degree of the paraffin. This can be explained by the fact that the shell of microcapsule reduced the thermal transfer efficiency due to the longer transfer path of shell compared with bare paraffin.

The corresponding phase change latent heats of paraffin and microcapsules are shown in Fig. 5d. The latent heats of paraffin and microcapsules can be calculated from the integral area of melting or crystallization peaks on the DSC curves. Clearly, the paraffin exhibits highest phase change temperature and latent heat during both melting and crystallization process. The melting and crystallization temperatures also increased at first and then decreased with increasing the GO contents, and they were all lower than those of paraffin. Comparing the latent heats of microcapsules with different GO content, we can find that the phase change temperature and latent heats of GO-5 was highest and were closest to those of paraffin, indicating a good phase change temperature-regulation performance. Cooling curves of paraffin and microcapsules were shown in Fig. S2† to study the phase change process. The results indicated that the cooling curves of GO-0, GO-3 and GO-7 were not significantly different due to the unobvious phase change process of lower content paraffin in microcapsules. While the cooling behavior of GO-5 was closest to that of paraffin. Such result was consistent with the data of DSC. The phase change performance of microcapsules demonstrated that paraffin was encapsulated successfully and the prepared microcapsules had temperature regulation properties.

The encapsulation ratio, the encapsulation efficiency and the thermal storage capability are important factors to evaluate the performance of phase change microcapsules, and they can be calculated by the results of the DSC measurements according to following equations, respectively.[19,43,44]

$$\text{Encapsulation ratio} = \frac{\Delta H_{\text{M}}}{\Delta H_{\text{Paraffin}}} \times 100\%$$

$$\text{Encapsulation efficiency} = \frac{\Delta H_{\text{m-M}} + \Delta H_{\text{c-M}}}{\Delta H_{\text{m-Paraffin}} + \Delta H_{\text{c-Paraffin}}} \times 100\%$$

$$\text{Thermal storage capability} = \frac{(\Delta H_{\text{m-M}} + \Delta H_{\text{c-M}})/R}{\Delta H_{\text{m-Paraffin}} + \Delta H_{\text{c-Paraffin}}} \times 100\%$$

where $\Delta H_{\text{-M}}$ and $\Delta H_{\text{-Paraffin}}$ are latent heats of microcapsules and paraffin, respectively. The subscript m and c represent melting and crystallization process, respectively. As shown in Table 2, the encapsulation ratio increased at first and then decreased with increasing the GO contents. The encapsulation ratio of GO-5 was the highest and reached to 31.98%. Consequently, the encapsulation ratio represents the effective performance of the paraffin in the microcapsules for heat energy storage, while the encapsulation efficiency is more rational to evaluate the efficiency of the microcapsule, because it involved both of the melting and crystallization processes. The encapsulation efficiency showed a similar trend to the encapsulation ratio, and the largest values appeared in GO-5. In our case, the encapsulation ratio and encapsulation efficiency of paraffin was not high due to a small ratio of paraffin to shell material compared to the literature.[19] The purpose is to achieve balance of phase change temperature regulation and humidity control by optimal ratio of core to shell.

The samples presented a thermal storage capability higher than 90% except GO-3, indicating that the encapsulated paraffin in microcapsules could store the latent heat effectively *via* phase change process.

Thermal durability of microcapsules

The thermal durability of microcapsules was investigated by thermal cycling test. A 10 thermal cycling test was performed to evaluate the phase change durability of microcapsule GO-5. The phase change temperature peaks and latent heat were recorded. Fig. 6a shows the DSC curves of the as-prepared GO-5 and after different thermal cycling test. The DSC curve of microcapsule GO-5 after 5 and 10 heating–cooling cycles was close to that of the as-prepared GO-5. There were almost no changes in the phase change temperature and slight decrease in the latent heat during melting process (see Fig. 6b and c). That is, it is acceptable in latent heat thermal energy storage applications. The microcapsules had a good thermal durability.

Thermal conductivity and leakage performance

Thermal conductivity is another important factor for evaluation of phase change microcapsules. In general, paraffin displays poor thermal conductivity, which could affect the thermal storage or release. Here, GO with outstanding thermal conductivity was introduced to improve the heat transmission of microcapsules. Thermal conductivity of the prepared microcapsules is shown in Fig. 7. Obviously, the thermal

Table 2 The phase change characteristics of paraffin and as-prepared microcapsules

Samples	ΔH_{c} (J g^{-1})	ΔH_{m} (J g^{-1})	Encapsulation ratio (%)	Encapsulation efficiency (%)	Thermal storage capability (%)
Paraffin	71.43	75.54	—	—	—
GO-0	11.51	14.31	18.94	17.57	92.76
GO-3	5.91	9.49	12.56	10.48	83.43
GO-5	18.83	24.16	31.98	29.25	91.47
GO-7	11.89	14.93	19.76	18.25	92.35

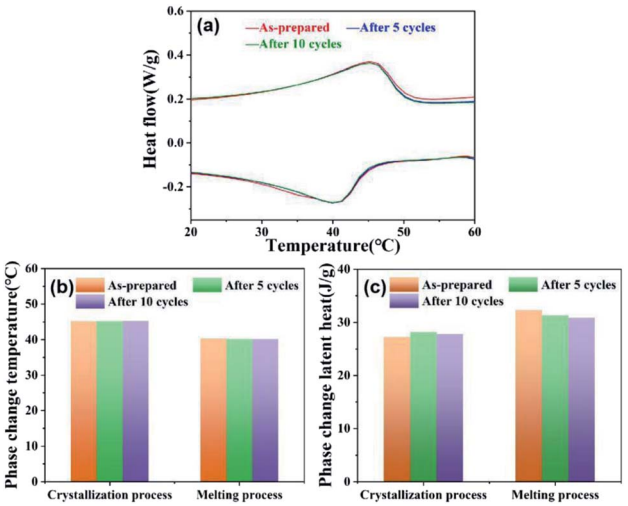

Fig. 6 (a) DSC curves of the as-prepared GO-5 and after different thermal cycling test, their corresponding (b) phase change temperature and (c) latent heat.

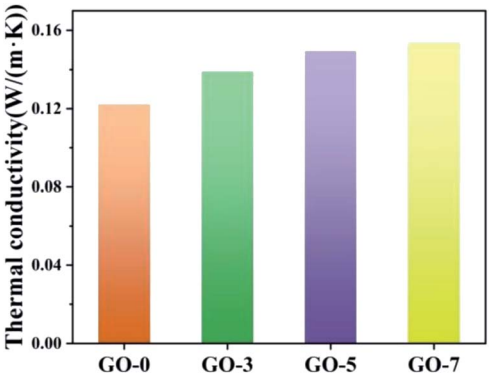

Fig. 7 Thermal conductivity of the prepared microcapsules.

conductivity of the microcapsules increased when the used GO contents increased from 0 to 7 mL (from GO-0 to GO-7) owing to the excellent thermal conductivity of GO. They were 0.1222, 0.1391, 0.1494 and 0.1538 W m^{-1} K^{-1} for GO-0, GO-3, GO-5 and GO-7, respectively.

The leakage of paraffin from microcapsules was measured at 50 °C for 24 h. Fig. 8a shows that the leakage ratios of GO-0, GO-3, GO-5 and GO-7 were 9.78%, 2.37%, 2.63% and 3.13%, respectively. The leakage ratios reduced by 75.8%, 73.1% and 68.0% for GO-3, GO-5 and GO-7 compared with GO-0. Obviously, the leakage-prevention of microcapsules was enhanced upon addition of GO. The increase of GO content had little effect on the improvement of leakage. This can be explained by the fact that the excessive GO had been electrostatically assembled with chitosan in the reaction solution instead of on the microcapsule shell. As a result, the leakage ratio was not further reduced with an increase in GO contents. As shown in insets of Fig. 8a, the melted paraffin in the microcapsule without GO (GO-0) could travel through the chitosan layer, while it would be inhibited for the microcapsules containing

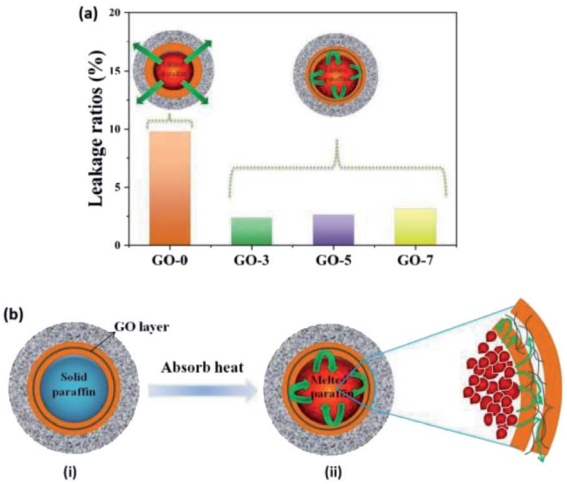

Fig. 8 (a) Leakage ratios and (b) schematic illustration of low leakage mechanism. The leakage ratios were reduced by the introduction of GO layer in the inner shell. When the environmental temperature is higher than the melting point of paraffin, paraffin inside microcapsules absorb heat and becomes liquefied paraffin, which will be prevented by GO sheet from leakage (from i to ii).

GO. Herein, GO nanosheets prevented paraffin from leakage during the melting process, showing a good screen effect. The mechanism of low leakage is shown in Fig. 8b. When the environmental temperature increased to the melting point, paraffin inside the microcapsules absorbed heat and changed into liquefied paraffin (from i to ii). The liquefied paraffin could be prevented by GO sheet from leakage, resulting in lower leakage ratios for microcapsules with GO. The detailed mechanism is shown in the right local enlarged image. The green arrows indicate the path of liquefied paraffin after absorb heat. The liquefied paraffin passed through the chitosan layer to GO sheet layer, but was blocked by GO, or a small amount of them diffused into GO sheets through a longer path. Therefore, the paraffin is difficult to escape from the core due to the barrier of GO layer in the inner shell.

Such a low leakage of paraffin by the introduction of GO is very important, because the porous shell with humidity regulation can be designed on the base of such a good phase change stability with low leakage of paraffin. That is, the dual regulation performance of temperature and humidity of microcapsules could be realized only by GO effectively reduce the leakage, which can ensure the feasibility in practical application.

Humidity regulation

The composition and structure of microcapsules' shell not only have an effect on the phase change paraffin, but also play a decisive role in the moisture adsorption and desorption properties. Humidity regulation materials can selectively absorb or desorb moisture according to the change of relative humidity and narrows the humidity fluctuation without any energy consumption.[45,46] Porous materials are considered the most promising humidity control materials. For the prepared microcapsules containing chitosan/GO/chitosan inner shell

and SiO_2 outer shell, the hydrophilic groups of chitosan and the surface of SiO_2, such as hydroxyl and amino, can adsorb moisture from air, which is beneficial to the adsorption of moisture. Furthermore, chemically precipitated SiO_2 shell formed loose mesoporous structure (Fig. 3), which endows the outer shell with a large specific surface area and can be served as channels for moisture adsorption and storage space. Therefore, the synergy of chitosan and SiO_2 shell contributed to the moisture adsorption, proved by the following humidity regulation performance.

The humidity regulation property was evaluated by moisture adsorption and desorption under the environments at different relative humidity. The equilibrium moisture contents are exhibited in Fig. 9a. The equilibrium moisture content increased with the increasing relative humidity for each microcapsule. The humidity regulation was mainly attributed to the diffusion and adsorption of moisture into the double shells of microcapsules, resulted from the hydrophilic groups in chitosan and porous SiO_2 shell. In addition, equilibrium moisture contents of microcapsules with GO were higher than that of microcapsule without GO. The moisture adsorption rates under different relative humidity in Fig. S3.† At higher relative humidity (RH = 75%, 84%, 97%), the moisture adsorption ratio of microcapsules with GO were also higher than that of the microcapsule without GO. The results demonstrated that the introduction of GO not only did not affect the moisture adsorption of microcapsules, but also resulting higher moisture adsorption rate at higher relative humidity of environment. This is because the hydrophilic groups (carboxyl, hydroxyl) of GO can adsorbed moisture from air due to the high humidity conditions.

In fact, both adsorption and release of moisture determined the humidity regulation. Fig. 9b shows the moisture desorption curves of the as-prepared microcapsules. The moisture desorption could be divided into two stages. The first stage occurred in the first 270 min at a faster release rate. Then the amount of moisture desorption kept constant from 270 min to 1080 min. The second stage started from 1080 min at a slower desorption rate. Comparing with the released moisture content of the two stages, we can find that most of the moisture was released at the first stage. It was calculated that 74.0%, 82.4%, 74.4% and 80.9% of the total moisture were released at the first stage for GO-0, GO-3, GO-5 and GO-7, respectively. Therefore, the first stage played a key role in the desorption process.

Fig. 9c exhibits the schematic illustration of the humidity regulation mechanism. The moisture diffused into the nanopores of SiO_2 shell, and then was adsorbed on its porous wall and stored in the SiO_2 shell due to the loose structure formed by the aggregation of nano-sized SiO_2 and hydrophilic groups. When the environmental relative humidity was lowered, the adsorbed moisture in the pores of SiO_2 would be released quickly (Fig. 9b Stage I).[47] During the constant stage (270–1080 min), the moisture adsorbed in the chitosan shell migrated slowly to the microcapsule surface, resulted in a slow moisture desorption rate. After 1080 min, the migrating moisture was released gradually with a slower rate (Fig. 9b Stage II). Such a moisture desorption process was beneficial to the stable humidity regulation according to the environmental humidity.

Moisture adsorption/desorption stability of microcapsule (GO-5) was characterized after repeated adsorption/desorption under the condition of RH = 97% and 32%, respectively. Fig. 10 shows the moisture content of microcapsule for 10 cycles of adsorption/desorption. The moisture content of microcapsules did not reduce significantly after 10 cycles, indicating a good stability. This result should be contributed to the special porous shell. Most of the moisture was physically adsorbed in the pores of SiO_2 shell. The physical adsorption made the

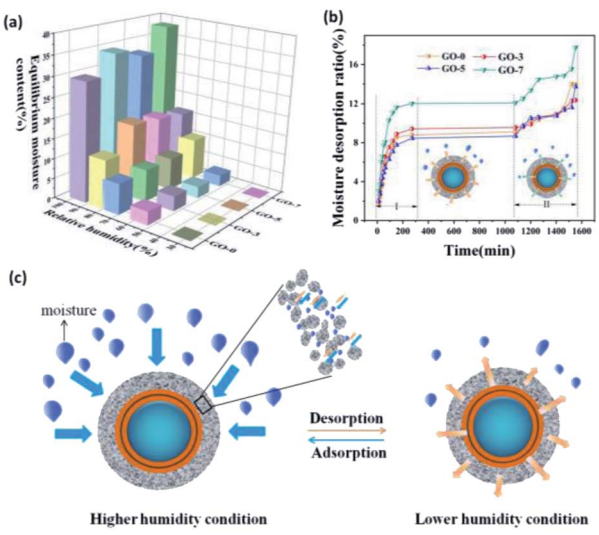

Fig. 9 (a) Equilibrium moisture contents of the prepared microcapsules, (b) moisture desorption curves of the moisture-saturated microcapsules and (c) schematic illustration of humidity regulation mechanism. The microcapsules shell adsorbs moisture from environment under higher humidity condition. Upon exposure to lower humidity environment, the moisture will be released. The moisture desorption process can be divided into two stages: (I) faster desorption: moisture desorption from the porous and loose SiO_2 shell; (II) slower desorption: moisture desorption from the chitosan inner shell.

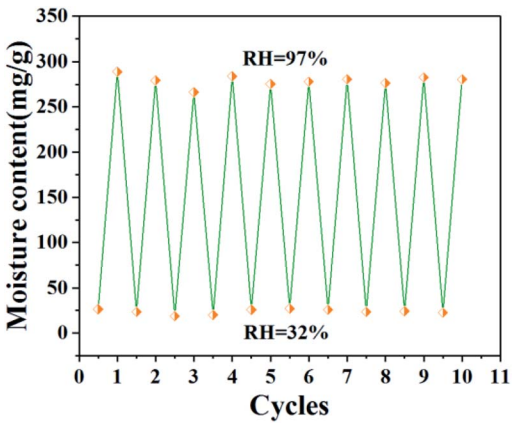

Fig. 10 Moisture content of microcapsule (GO-5) under the condition of RH = 32% and 97% for 24 h after 10 cycles.

moisture easy to be desorbed when the humidity changed even after repeatedly adsorption/desorption.

These results confirmed that the as-constructed single-core–double-shells microcapsules successfully achieved the temperature–humidity dual regulation and low leakage, indicating that artfully designing the core and shell of microcapsules and combining their functions can realize the multi-functional and multi-factors regulation. Performance comparison of the as-prepared microcapsules with both the main raw materials (paraffin, SiO_2 and chitosan) and the materials reported in literature was shown in Table S1.† The moisture adsorption of our microcapsules was much better than those of the raw materials. In addition, our single-core–double-shell microcapsules had the ability to regulate the temperature and humidity simultaneously, which was superior to the similar core–shell paraffin@SiO_2 microcapsules with single phase change temperature regulation.[18]

The temperature and humidity regulation in simulated environment

The as-prepared microcapsules have potential applications in building materials to regulate the indoor temperature and humidity, or as an additive in clothing materials, playing a role in keeping warm and moisture permeability to improve wearing comfort.

In order to investigate the practical performance of microcapsule, the sample GO-5 was placed in a tiny container in the real laboratory environment with a relative constant temperature and a low humidity, showing a weak regulation ability for temperature and humidity (Fig S4†). The reason is that laboratory temperature has not reached the phase change temperature of the paraffin in the core of microcapsule and the sample could not adsorb moisture in the low humidity of the laboratory environment. To further illustrate the performance, we did the experiment again in a temperature-changed (25–45 °C) and high humidity (40–75%) environment. The results in Fig. 11 show that the temperature and humidity for both of the sample GO-5 and the blank increased significantly as the temperature and humidity of environment went up. It also can be found that the increase in temperature and humidity of the sample was slower than that of the blank. Fig. 11a shows the temperature regulation in the range of 25–45 °C. Obviously, the temperature change was slower compared to the blank around the phase change temperature of paraffin (~40 °C) due to the endothermic/exothermic of paraffin during phase change process. When the temperature difference of the environment was set at 20 °C, the measured change of the blank was 19.9 °C which was consistent with the given temperature difference. However, the temperature change of 18.6 °C was obtained for the sample GO-5, indicating temperature regulation performance of the constructed microcapsules. Here the relatively weak temperature regulation is because the content of paraffin for GO-5 was 31.98%, which was much lower than the content reported in the literature.[14,18,48] This indicates that increasing the encapsulation ratio of paraffin can improve the temperature regulation performance. For humidity regulation (Fig. 11b), the humidity change of the blank was 35.8%, which was also consistent with the given humidity difference (RH: 40–75%). However, a humidity change of 28.8% for the sample was acquired, which was obviously lower than the given humidity difference obviously small of the sample. The reason is that our microcapsules can adsorb moisture and cause a lower humidity of the environment, indicating their excellent humidity regulation performance. The above-results demonstrated that the as-prepared microcapsule could remain stable temperature and relative humidity when the ambient temperature and humidity changed.

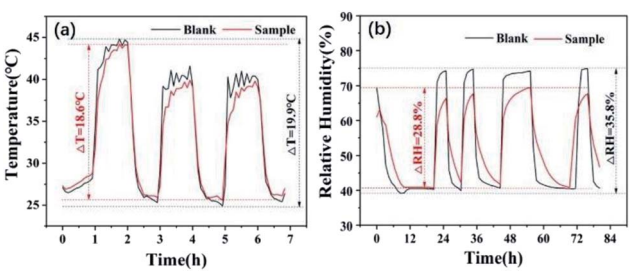

Fig. 11 The temperature and humidity regulation of GO-5 in simulated environment.

Conclusion

We developed a single-core–double-shell phase change microcapsule based on paraffin core and chitosan/GO/chitosan–SiO_2 shell *via* electrostatic assembly and chemical precipitation method. The microcapsules were regularly spherical morphology and exhibited good thermal energy storage, high thermal conductivity and temperature–humidity dual regulation with low leakage. The introduction of GO also improved the moisture adsorption performance at higher relative humidity. More than 74.0% of the total moisture were released from the loose and porous SiO_2 outer shell, which played a key role in the desorption process. More importantly, the as-prepared microcapsule exhibited good thermal durability and moisture adsorption/desorption stability. This type of single-core–double-shell multifunctional microcapsule has potential applications in the fields of building materials and leather/textile coatings.

Conflicts of interest

There are no conflicts to declare.

Acknowledgements

This work was supported by National Natural Science Foundation of China (grant no. 21663032); The Open Project of Shaanxi Collaborative Innovation Center of Industrial Auxiliary Chemistry & Technology (grant no. XTKF-2019-01); Natural Science Fundamental Research Program of Yan'an University (grant no. YDBK2015-11, YDQ2017-15); Key Laboratory project of Education Department of Shaanxi Province (grant no. 16JS120); College Students Innovation and Entrepreneurship Training Program of Shaanxi Province (no. D2018011).

References

1 S. E. Kalnaes and B. P. Jelle, *Energ. Build.*, 2015, **94**, 150–176.
2 Z. Chen, D. Su, M. Qin and G. Fang, *Energ. Build.*, 2015, **86**, 1–6.
3 F. Salaun, in *Developments in heat transfer*, ed. B. Marco Aurelio Dos Santos, 2011.
4 H. Maeda and E. H. Ishida, *J. Am. Ceram. Soc.*, 2009, **92**, 2125–2128.
5 J. Giro-Paloma, M. Martínez, L. F. Cabeza and A. I. Fernandez, *Renewable Sustainable Energy Rev.*, 2016, 531059–531075.
6 Y. Yoo, C. Martinez and J. P. Youngblood, *ACS Appl. Mater. Interfaces*, 2017, **9**, 31763–31776.
7 J. F. Niu, H. Liu, X. D. Wang and D. Z. Wu, *ACS Appl. Mater. Interfaces*, 2019, **11**(37), 644–664.
8 T. Do, Y. G. Ko, Y. Chun and U. S. Choi, *ACS Sustainable Chem. Eng.*, 2015, **32**, 874–881.
9 H. Wei, F. F. He, Y. S. Li, Q. P. Zhang, Y. L. Zhou, H. J. Yan, R. He, J. H. Fan and W. B. Yang, *ACS Sustainable Chem. Eng.*, 2019, **7**, 18854–18862.
10 X. Q. Song, Y. X. Li and J. W. Wang, *Adv. Mater. Res.*, 2013, **815**, 367–370.
11 R. Yang, Y. Zhang, X. Wang, Y. Zhang and Q. Zhang, *Sol. Energy Mater. Sol. Cells*, 2009, **93**, 1817–1822.
12 Y. T. Fang, T. Zou, X. H. Liang, S. F. Wang, X. Liu, X. N. Gao and Z. G. Zhang, *ACS Sustainable Chem. Eng.*, 2017, **5**, 3074–3080.
13 F. Y. Jiang, X. D. Wang and D. Z. Wu, *Appl. Energy*, 2014, **134**, 456–468.
14 T. Y. Wang, S. F. Wang, R. L. Luo, C. Y. Zhu, T. Akiyama and Z. G. Zhang, *Appl. Energy*, 2016, **171**, 113–119.
15 X. Y. Zhang, X. D. Wang and D. Z. Wu, *Energy*, 2016, **111**, 498–512.
16 N. Sun and Z. G. Xiao, *Energy Fuels*, 2017, **31**, 10186–10195.
17 Z. H. Chen, J. C. Wang, F. Yu, Z. G. Zhang and X. N. Gao, *J. Mater. Chem. A*, 2015, **3**, 11624–11630.
18 R. L. Luo, S. F. Wang, T. Y. Wang, C. Y. Zhu, T. Nomura and T. Akiyama, *Energ. Build.*, 2015, **108**, 373–380.
19 Z. N. Jiang, W. B. Yang, F. F. He, C. Q. Xie, J. H. Fan, J. Y. Wu and K. Zhang, *ACS Sustainable Chem. Eng.*, 2018, **6**, 5182–5191.
20 L. Zhang, W. B. Yang, Z. N. Jiang, F. F. He, K. Zhang, J. H. Fan and J. Y. Wu, *Appl. Energy*, 2017, **197**, 354–363.
21 H. Liu, X. D. Wang and D. Z. Wu, *ACS Sustainable Chem. Eng.*, 2017, **5**, 4906–4915.
22 S. Stankovich, D. A. Dikin, R. D. Piner, K. A. Kohlhaas, A. Kleinhammes, Y. Jia, Y. Wu, S. T. Nguyen and R. S. Ruoff, *Carbon*, 2007, **45**, 1558–1565.
23 L. F. Wei, W. B. Zhang, J. Z. Ma, S. L. Bai, Y. J. Ren, C. Liu, D. Simion and J. B. Qin, *Carbon*, 2019, **149**, 679–692.
24 W. B. Zhang, J. Z. Ma, D. G. Gao, C. M. Li, Y. X. Zhou, J. Zha and J. Zhang, *Prog. Org. Coat.*, 2016, **94**, 9–17.
25 H. Yang, Y. Liu, X. F. Kong, W. H. Chen and C. Q. Yao, *J. Cent. South Univ.*, 2018, **25**, 2387–2398.
26 L. J. Shang and L. Dong, *J. Build. Mater.*, 2015, **18**, 428–432.
27 J. L. Shang, S. Wang and L. Dong, *Journal of Functional Materials*, 2013, **44**, 1141–1144.
28 H. Zhang, X. J. Huang, Z. F. Zong and X. Y. Liu, *Chin. J. Mater. Res.*, 2016, **30**, 418–426.
29 Z. Chen, M. H. Qin and J. Yang, *Energ. Build.*, 2015, **106**, 175–182.
30 Z. Chen and M. H. Qin, *Appl. Therm. Eng.*, 2016, **98**, 1150–1157.
31 L. Jiang, Y. B. Li, S. Yao and Z. H. Zhou, *Journal of Functional Materials*, 2015, **16**, 16119–16124.
32 C. J. Shih, S. Lin, R. Sharma, M. S. Strano and D. Blankschtein, *Langmuir*, 2012, **28**, 235–241.
33 S. He, J. M. Liang, H. L. Hu, J. N. Yuan, J. B. He and Z. F. Ni, *Mater. Rev.*, 2016, **30**, 1–5.
34 K. Akamatsu, M. Ogawa, R. Katayama, K. Yonemura and S. Nakao, *Colloids Surf., A*, 2019, **567**, 297–303.
35 K. S. W. Sing, D. H. Everett, R. A. W. Haul, L. Moscou, R. A. Pierotti, J. Rouquerol and T. Siemieniewska, *Pure Appl. Chem.*, 1985, **57**, 603–619.
36 Q. S. Lian, Y. Li, A. A. S. Sayyed, J. Cheng and J. Y. Zhang, *ACS Sustainable Chem. Eng.*, 2018, **6**, 3375–3384.
37 E. Murugan and K. Kumar, *Anal. Chem.*, 2019, **91**, 5667–5676.
38 B. X. Li, T. X. Liu, L. Y. Hu, Y. F. Wang and L. N. Gao, *ACS Sustainable Chem. Eng.*, 2013, **1**, 374–380.
39 P. Kolhe and R. M. Kannan, *Biomacromolecules*, 2003, **4**, 173–180.
40 L. F. Wei, J. Z. Ma, W. B. Zhang, C. Liu and Y. Bao, *Prog. Org. Coat.*, 2018, **122**, 64–71.
41 P. J. Han, L. X. Lu, X. L. Qiu, Y. L. Tang and J. Wang, *Energy*, 2015, **91**, 531–539.
42 X. Y. Zhang, X. D. Wang and D. Z. Wu, *Energy*, 2016, **111**, 498–512.
43 B. X. Li, T. X. Liu, L. Y. Hu, Y. F. Wang and L. N. Gao, *ACS Sustainable Chem. Eng.*, 2013, **1**, 374–380.
44 T. T. Qian, J. H. Li, H. W. Ma and J. Yang, *Sol. Cells*, 2015, **132**, 29–39.
45 X. P. Liu, Z. Chen, G. Yang, Z. T. Zhang and Y. F. Gao, *ACS Omega*, 2019, **4**(9), 13896–13901.
46 X. P. Liu, Z. Chen, G. Yang and Y. F. Gao, *Ind. Eng. Chem. Res.*, 2019, **58**, 7139–7145.
47 Y. Zhang, Z. Z. Jing, X. W. Fan, J. J. Fan, L. Lu and E. H. Ishida, *Ind. Eng. Chem. Res.*, 2013, **52**, 4779–4786.
48 Y. Zhang, K. H. Wang, W. Tao and D. X. Li, *Constr. Build. Mater.*, 2019, **224**, 48–56.